Experimental and Theoretical Investigation of Mixing in a Bottom Gas-Stirred Ladle

Jun Aoki, Brian G. Thomas
Dept. of Mechanical & Industrial Engineering
University of Illinois at Urbana-Champaign
1206 West Green Street
Urbana, IL 61801
Tel.: 217-333-6919
Fax: 217-244-6534
E-mail: junaoki@uiuc.edu, bgthomas@uiuc.edu

Jörg Peter, Kent D. Peaslee
Dept. of Metallurgical Engineering
University of Missouri-Rolla
1870 Miner Circle, 218 McNutt Hall
Rolla, MO 65409-0340
Tel.: 573-341-4714
Fax: 573-341-6934
Email: jjpeter@umr.edu, kpeaslee@umr.edu

Key words: Steelmaking, Ladle refining, Off-centered gas injection, Multiphase flow modeling, Ferroalloy addition, Ferroalloy melting, Mixing

INTRODUCTION

Gas stirred ladle refining is widely used in steelmaking to homogenize temperature and chemical composition, as well as to remove inclusions. Accurate ability to predict the mixing time is important because it determines the operation time needed to ensure homogeneity. In addition, it can provide further insight into optimizing process parameters for developing new practices and vessel designs. For example, the development of a new process for continuous steelmaking needs computational models with sufficient accuracy to validate the process prior to full-scale pilot-plant trials and commercialization.

In this paper, a fundamental investigation is undertaken to quantify mixing in a gas-stirred ladle with off-centered bottom injection. Industrial trials in a Ladle Metallurgy Furnace (LMF) were performed to investigate the time-dependent change in concentration of various elements in the steel during the addition of a Silicomanganese (SiMn) ferroalloy into unkilled steel. The measurements were used to validate a computational model featuring the simulation of the three-dimensional multi-phase fluid-flow, and the simulation of the ferroalloy addition, transport, melting, and mixing.

This work is a first step to quantify metallurgical phenomena during steel treatment at the LMF. In addition, the results of this study will be combined in future work with other experiments and simulations to design a fully continuous steelmaking process.

EXPERIMENTAL PROCEDURE – INDUSTRIAL TRIAL

The first set of experiments included temperature and composition measurements during and after ferroalloy additions at a LMF station for eight heats of a common structural steel grade. The argon flow rate, the initial and final temperatures, the initial and final calculated oxygen concentrations and the manganese recovery are listed in Table I. The manganese recoveries of the eight heats ranged between 91% and 98% and the initial oxygen concentration of these heats ranged between 380 ppm and 1055 ppm. Heat 1 had the highest alloy recovery and the lowest initial oxygen concentration, and therefore was deemed the most accurate for comparing the industrial data and the computer-model predictions, described later. The detailed operational conditions for Heat 1 are described in this section. The results for Heat 2 were used to investigate the effect of superheat on alloy melting and mixing. The experimental conditions during Heat 2 were generally similar to Heat 1, except that the gas flow rate was lower, reducing the flow velocities.

Table I Operational conditions, oxygen change, and manganese recovery in the eight heats

Heat	Ar flow rate (Nm^3/min)	Temperature (°C)		Oxygen (ppm)		Mn recovery (%)
		Initial	Final	Initial	Final	
1	0.170	1551	1516	380	20	97.8
2	0.113	1590	1557	909	30	93.0
3	0.113	1578	1541	415	25	96.6
4	0.113	1566	1529	1055	23	91.1
5	0.113	1605	1568	810	33	95.1
6	0.113	1586	1564	734	32	95.6
7	0.170	1577	1533	840	24	94.7
8	0.170	1577	1552	735	29	95.8

Possible reasons for the high alloy recovery of Heat 1 are the low slag reactivity and low initial oxygen content in the steel, owing to the low temperature of the steel and the high initial carbon content (0.051%). The temperature was 1551°C at the beginning of the measurements and decreased to 1516°C by the end of the trial, which was lower than steel temperatures of the other seven heats. The liquidus decreased from 1529°C to 1518°C during the experiment because of the alloy addition. This corresponds to a drop of the superheat from 22°C to 0°C. The other seven heats had similar liquidus temperatures; but their steel temperatures were higher, averaging 1566°C.

The size and shape of the ladle, the location of the porous plug, the location of the ferroalloy addition, and the sampling location are illustrated in Figure 1. Heat 1 was the twenty-first heat of the ladle refractory campaign and the sixth heat on the alumina porous plug. The diameter of the porous plug at the steel/refractory interface was 113 mm. It was estimated that the slag layer on the ladle had an average thickness of approximately 35 mm, with a freeboard distance of ~0.3m below the top of the ladle. The sampling location was approximately 300 mm below the slag/air surface, near the location of the ferroalloy addition (see Figure 1). Efforts were made to take the 24 composition samples and the two temperature measurements from the same location. On average, samples were taken every 22 seconds. The surface of the liquid was disturbed due to the stirring action of the argon gas with resulting surface waves of approximately 200 mm to 300 mm high. This was observed to mix the slag and the steel at the steel slag interface.
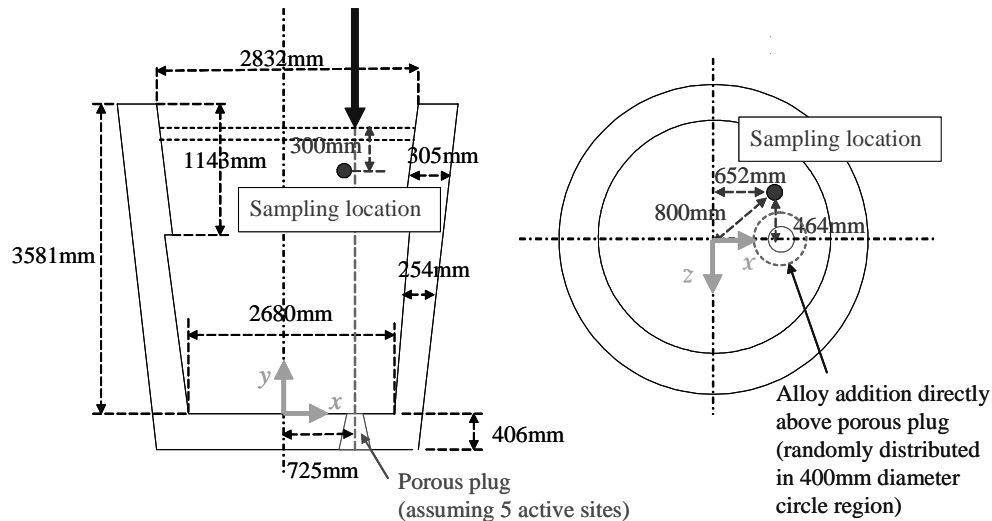

Figure 1 Schematic illustration of the size and shape of the ladle (130 tonnes nominal capacity), including the porous plug, ferroalloy addition location, and sampling location

The argon flow rates were 0.17 and 0.113 Nm3/min at pressures of 448 and 269 kPa gage with an estimated maximum leakage of less than 5% for Heat 1 and 2 respectively. New couplings were recently installed and the connections were checked for tightness before sampling started. The stirring gas contained 99.99% argon, less than 20 ppm nitrogen, and less than 5 ppm oxygen.

It took 37 seconds to add the 1823.44 kg of SiMn ferroalloy to the steel. The ferroalloy entered the steel directly above the off-center porous plug where the slag layer is thinner than in the rest of the top surface (eye). It was estimated that the velocity of the ferroalloy pieces at the time of their entry into the liquid steel was similar to the velocity of pieces after a vertical free fall of approximately two meters (6 m/s). Ninety weight percent of the ferroalloy was between 13 mm and 64 mm in size, five weight percent between 64 mm and 76 mm, and the remaining 5 percent was fines. A normal size distribution of the ferroalloy was assumed. Furthermore, the ferroalloy particles did not contain foreign matter (e.g. dirt) and it was dense without any visible porosity. The chemical composition of the SiMn ferroalloy is detailed in Table II.

Table II Chemical composition of SiMn ferroalloy

Element	Mn	Si	C	P	S	Moisture	Fe
%	71.8	16.3	1.9	0.45	0.007	0.07	balance

The concentration changes of manganese, silicon, and carbon in the steel in response to the SiMn additions in Heat 1 and Heat 2 are plotted in Figure 2. Oscillating concentration variations were observed in all heats. However, the first small concentration drop at the end of the ferroalloy addition time seen in the left graph in Figure 2 was observed only in Heat 1. The steel samples were analyzed with a spectrometer. The phosphorus content of the steel increased from 0.010% to 0.020% during the experiment. The initial oxygen content was calculated based on the carbon concentration of the steel, and the final oxygen concentration was calculated based on the silicon concentration and the temperature of the steel.[1] The slag samples were taken with a spoon and analyzed using X-ray Fluorescence. The initial and final slag compositions and slag masses in Heat 1 are reported in Table III. It should be noted that the power was off and the electrodes were raised during the entire experiment, eliminating the potential for carbon pick-up.

Table III Initial and final slag composition and calculated mass

Component	CaO	SiO$_2$	Al$_2$O$_3$	MgO	MnO	FeO	Mass
Initial wt%	44.0	21.9	1.3	13.5	3.4	14.2	570 kg
Final wt%	38.7	28.8	1.3	16.6	8.8	4.8	645 kg

(The balance to 100% is other slag components such as phosphates, sulfides, and titania.)

A mass balance was performed to calculate the initial and final steel and slag mass and to quantify the alloy loss. In addition, the amount of refractory loss due to slag line erosion during the time between the two slag samples was calculated. For Heat 1, the calculated steel mass was 110.1 tonnes (metric tons) before the ferroalloy additions and 111.9 tonnes after the ferroalloy additions, closely matching the average tap weight of 111 tonnes at this facility. The calculated slag mass increased from 570 kg before the additions to 645 kg after the final chemistry sample. These slag masses correlate well to the estimated observed average slag thickness of 35 mm. An estimated 33.6 kg of refractory was lost within 610 seconds between the two slag samples.

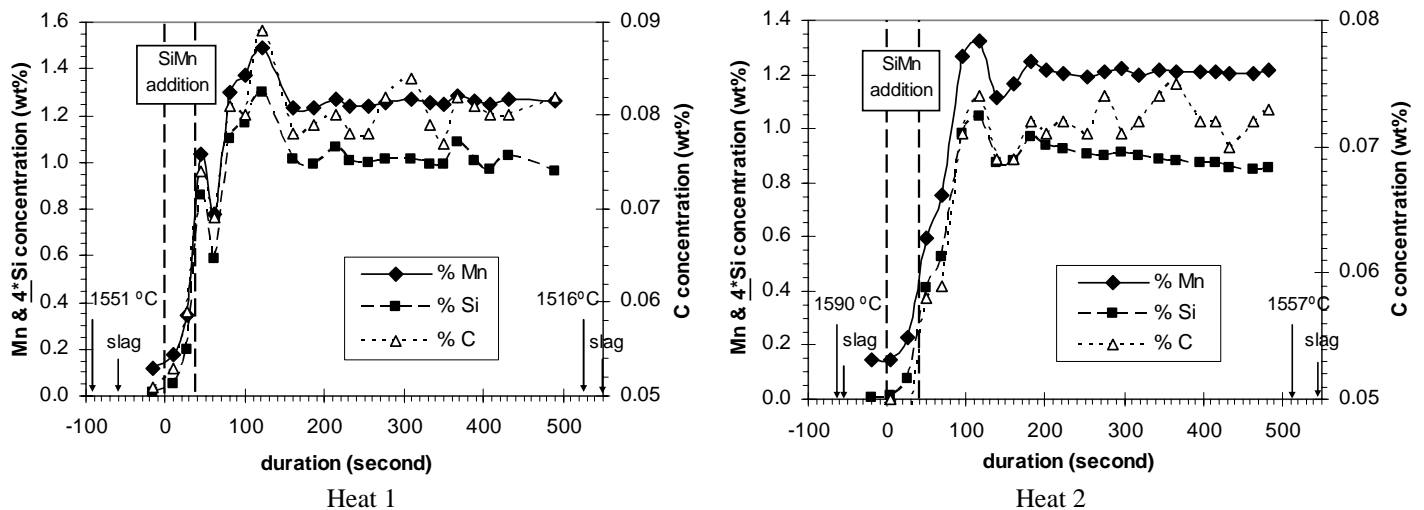Heat 1   Heat 2

Figure 2 Steel concentrations of Mn, Si, and C during the experiment.
Times for temperature and slag samples are also shown.

Table IV Alloy losses and resulting effects on steel composition, including effects from slag line erosion

	Alloy loss		Change in steel concentrations	
	Mass of element	Percent of element	due to Oxidation	due to Erosion
	kg	%	wt % steel	wt % steel
Mn	27	2.1	- 0.025	n/a
Si	27	9.1	- 0.025	n/a
C	2	5.8	- 0.002	+ 0.003
Total alloy	56	3.1	-	-

The mass balance calculations were based on the mass of the ferroalloy, the mass fraction of manganese, silicon, and carbon in the ferroalloy; the initial and final manganese, silicon, and carbon concentrations in the steel; the calculated initial and final oxygen concentration in the steel, and the initial and final concentrations of the slag components (MnO, SiO$_2$, MgO, CaO, FeO). Intentionally, no fluxes were added to the slag during the experiment. As a result, the mass of lime (CaO) in the slag was kept constant. The refractory of the slag line was MgO-C (10% C). The calculated alloy losses are summarized in Table IV. The results for Heat 2 were generally similar, except that the gas flow rate was only 0.113 Nm^3/min, so flow velocities and mixing were slower.

COMPUTATIONAL MODEL

The model consists of two calculation steps. First, the three-dimensional multi-phase flow field in the vessel is calculated based on the flow caused by the jet of injected gas. Secondly, the ferroalloy addition, melting and dissolution are modeled.

Flow Model

A single set of Navier-Stokes equations is solved for the liquid phase and a discrete-phase model is used for the gas phase. The liquid phase equations are as follows.

Continuity equation:
$$\nabla \cdot \underline{u} = 0 \tag{1}$$

Momentum conservation:
$$\rho\left(\frac{\partial \underline{u}}{\partial t} + \underline{u} \cdot \nabla \underline{u}\right) = -\nabla p + \nabla(\mu + \mu_t)\nabla \underline{u} - \rho \underline{g} + \sum_{i=1}^{N_b} F_{D,i}\left(\underline{u} - \underline{u}_{b,i}\right)Q_b dt \tag{2}$$

where $\underline{u}$ is the time-averaged fluid velocity, ρ is the density of liquid steel, p is the pressure, μ is the molecular viscosity of liquid steel, μ_t is the turbulent viscosity, $\underline{g}$ is the gravitational acceleration, N_b is the total number of bubbles in the domain, $F_{D,i}$ is the drag force from each bubble as described later, $\underline{u}_{b,i}$ is the time-averaged velocity of each bubble, and Q_b is the gas flow rate. The last term of equation (2) represents a momentum source due to bubble flotation, found by summing the local contributions from each individual bubble in the domain. The subscript i refers to the number of each bubble.

The standard k-ε model is used to model turbulence in the liquid phase.

Turbulent viscosity, μ_t:
$$\mu_t = C_\mu \rho \frac{k^2}{\varepsilon} \tag{3}$$

Transport equation of turbulent kinetic energy in the liquid phase, k:
$$\rho\left(\frac{\partial k}{\partial t} + \underline{u} \cdot \nabla k\right) = \nabla\left(\frac{\mu_t}{\sigma_k}\nabla k\right) + G_k - \rho\varepsilon \tag{4}$$

Transport equation of dissipation rate of turbulent kinetic energy in the liquid phase, ε:
$$\rho\left(\frac{\partial \varepsilon}{\partial y} + \underline{u} \cdot \nabla \varepsilon\right) = \nabla\left(\frac{\mu_t}{\sigma_\varepsilon}\nabla \varepsilon\right) + C_1 \frac{\varepsilon}{k}G_k - C_2\rho\frac{\varepsilon^2}{k} \tag{5}$$

4

where the generation of turbulent kinetic energy, G_k:

$$G_k = \mu_t \left(\frac{\partial u_i}{\partial x_j} + \frac{\partial u_j}{\partial x_i} \right) \frac{\partial u_i}{\partial x_j} \tag{6}$$

and where C_1, C_2, $C\mu$, σ_k, σ_ε are the empirical constants whose values are 1.44, 1.92, 0.09, 1.0 and 1.3 respectively.

The Ar gas bubbles are treated as discrete second phase particles. The trajectory of each bubble is calculated in each time step according to the buoyancy force and the drag force between the bubble and the flow field. Thus, the flow and the bubble trajectory equations are fully coupled. Additionally, the chaotic effect of turbulence on the trajectories is considered using the random walk model as described later. The equations for the bubble trajectories and drag forces are as follows.

Bubble trajectories:

$$\underline{x}_{b,i} = \int \left(\underline{u}_{b,i} + \underline{u}'_{b,i} \right) dt \tag{7}$$

Force balance on each bubble:

$$\frac{d\underline{u}_{b,i}}{dt} = F_{D,i} \left(\underline{u} - \underline{u}_{b,i} \right) - \frac{(\rho - \rho_b)}{\rho_b} \underline{g} \tag{8}$$

Drag force on each bubble:

$$F_{D,i} = \frac{18\mu}{\rho_b d_{b,i}^2} \frac{C_{D,i} \, \mathrm{Re}_i}{24} \tag{9}$$

Particle Reynolds number:

$$\mathrm{Re}_i = \frac{\rho d_{b,i} \left| \underline{u} - \underline{u}_{b,i} \right|}{\mu} \tag{10}$$

Drag coefficient:

$$C_{D,i} = \frac{24}{\mathrm{Re}_i} \left(1 + b_1 \, \mathrm{Re}_i^{b_2} \right) + \frac{b_3 \, \mathrm{Re}_i}{b_4 + \mathrm{Re}_i} \tag{11}$$

where $\underline{x}_{b,i}$ is the position of each bubble, $\underline{u}'_{b,i}$ is the fluctuation velocity of each bubble due to turbulence, ρ_b is the density of the bubble, $d_{b,i}$ is the diameter of each bubble, and $C_{D,i}$ is its drag coefficient. In equation (11), $b_1 \sim b_4$ are parameters in the non-spherical particle drag model by Haider and Levenspiel.[2]

$$\begin{aligned}
b_1 &= \exp(2.3288 - 6.4581\phi + 2.4486\phi^2) \\
b_2 &= 0.0964 + 0.5565\phi \\
b_3 &= \exp(4.905 - 13.8944\phi + 18.4222\phi^2 - 10.2599\phi^3) \\
b_4 &= \exp(1.4681 + 12.2584\phi - 20.7322\phi^2 + 15.8855\phi^3)
\end{aligned} \tag{12}$$

where ϕ is the shape factor, defined as

$$\phi = \frac{s}{S} \tag{13}$$

where s is the surface area of a sphere having the same volume as the particle, and S is the actual surface area of the particle.

The bubble size and shape are estimated using the following equations. The shape of the bubble is assumed to be spheroidal with uniform size. This simplification allows a single set of discrete particle equations to model the gas phase.

Bubble size is characterized by its equivalent diameter, using the empirical correlation with flow rate by Johansen and Boysan:[3]

$$d_{b,i} = 0.35 \left(\frac{Q_b^2}{g} \right)^{0.2} \tag{14}$$

Bubble shape is given by its eccentricity e, the ratio of the length between the shorter axis and the longer axis, as estimated from measurements in various media by Wellek et al.:[4]

$$e = 1 + 0.163 \text{Eo}^{0.757} \tag{15}$$

$$\text{Eo} = \frac{d_{b,i}^2 g (\rho - \rho_b)}{\sigma} \tag{16}$$

where Eo is the Eotvos number which corresponds to the ratio between the buoyancy force and the surface tension force, and σ is the surface tension of the fluid.

The fluctuating component of the particle velocity is found according to the local level of turbulent kinetic energy using the turbulent random walk model as follows:

$$\underline{u}'_{b,i} = \varsigma \sqrt{\frac{2k}{3}} \underline{e}_R \tag{17}$$

where ς is a random number uniformly distributed between 0 and 1, and $\underline{e}_R$ is a unit vector in a random direction. The fluctuation velocity is kept the same during the following random eddy lifetime τ_e.

$$\tau_e = -C_L \frac{k}{\varepsilon} \log_{10} r \tag{18}$$

where r is a random number uniformly distributed between 0 and 1, and C_L is an empirical constant (=0.15).

Ferroalloy Model

Next, the ferroalloy addition, transport, melting and mixing are modeled. In the experimental study, SiMn ferroalloy is added from above the surface of the stirring ladle. Thus, the ferroalloy addition is first treated as discrete second-phase particles with a common initial velocity added into the flow field computed based on stirring alone. Then, after some melting time and distance traveled through the flow field, each ferroalloy particle disappears and turns into a mass source of liquid solute that diffuses through the molten steel. In this study, manganese is the only solute considered.

Ferroalloy particle transport is calculated using the same equations as those for Ar bubbles (7)~(11), except that the ferroalloy particle is assumed to be spherical and the following equation for the drag coefficient is used.

$$C_D = a_1 + \frac{a_2}{\text{Re}} + \frac{a_3}{\text{Re}^2} \tag{19}$$

where the constants a_1, a_2, and a_3 are given by Morsi and Alexander.[5]   For these calculations, the liquid steel flow field is fixed. Thus, the coupling due to momentum exchange from the ferroalloy particles to the flow field (the last term of equation (2)) is ignored.

A solidified steel shell is formed around the surface of the ferroalloy particle when it first enters into the molten steel. This initially prevents any alloy mixing. Then, as the ferroalloy particle is heated by the surrounding liquid, the steel shell melts and finally disappears. Because the melting point of SiMn (1215°C) is much lower than that of steel, the ferroalloy particle should be fully liquid when the steel shell disappears. Thus, the molten ferroalloy is suddenly introduced into the liquid where it starts to diffuse. The time when this occurs matches the duration of the solidified steel shell, which is modeled by Zhang and Oeters.[6]

$$t_1 = \frac{C_{pA} \rho_A d_A}{\pi h} \frac{T_s - T_0}{T_M - T_s} \tag{20}$$

where t_1 is the shell existence time, C_{pA} is the specific heat of ferroalloy, ρ_A is the density of ferroalloy, d_A is the diameter of ferroalloy particle, h is the heat transfer coefficient at the surface of the ferroalloy particle, T_s, T_M and T_0 are the solidification temperature of the melt, the temperature of the melt and the initial temperature of the ferroalloy particle respectively.

The heat transfer coefficient h is estimated from the Nusselt number Nu, derived from the Reynolds number Re and the Prandtl number Pr of the flowing steel using the following correlation by Whitaker.[7]

$$\text{Nu} = \frac{d_A h}{k_M} \tag{21}$$

6

$$\mathrm{Nu} = 2 + (0.4\,\mathrm{Re}^{1/2} + 0.06\,\mathrm{Re}^{2/3})\,\mathrm{Pr}^{0.4} \tag{22}$$

$$\mathrm{Re} = \frac{\rho d_A \left| \underline{u} - \underline{u}_A \right|}{\mu}, \quad \mathrm{Pr} = \frac{C_{pM}\mu}{k_M} \tag{23}$$

where $\underline{u}_A$ is the velocity of the ferroalloy particle, $C_{p,M}$ is the heat capacity of the molten steel, and k_M is the thermal conductivity of the molten steel.

As the ferroalloy particles melt, the species transport model applies. The turbulent diffusion of the ferroalloy element (Mn in this case) is calculated by solving the following equation.

$$\frac{\partial}{\partial t}(\rho C_M) + \nabla \cdot (\rho \underline{u} C_M) = \nabla \cdot \left(\rho D_M + \frac{\mu_t}{Sc_t} \right) \nabla C_M \tag{24}$$

where C_M is the mass fraction of the solute, D_M is the diffusion coefficient of the solute, and Sc_t is the turbulent Schmidt number which is set to 0.7.

COMPUTATIONAL DOMAIN AND BOUNDARY CONDITIONS

The ladle shown in Figure 1 is modeled as a complete three dimensional computational domain of 130 tonnes, based on filling the ladle in Fig. 1 to a depth of 3.277m, leaving a freeboard of 0.3m. Argon gas is injected through a porous plug set at the bottom of the ladle. Five active sites generating Ar bubbles are assumed at the surface of the porous plug.

Substituting the operational Ar flow rate Q_b=5.055×10^{-3}kg/s (0.17m^3/min) into equation (14), the mean bubble diameter is estimated to be 28.2mm. From equations (15) and (16), e is estimated as 3.61 and the shape factor ϕ in the equation (13) is obtained as ϕ=0.736.

SiMn containing 71.8 wt% manganese is used as the ferroalloy. For simplicity, the diameter of each ferroalloy particle is assumed to be 30mm. The ferroalloy is added at a constant rate of 59.85 kg/s for 37 seconds. Ferroalloy transport, melting and mixing calculations are continued until 300 seconds after the starting time. As mentioned in the experimental section, the ferroalloy is added in a 400mm diameter circle region centered in the eye above the porous plug. The initial velocity of each ferroalloy particle at the steel surface is set to 6.26 m/s vertically downward, corresponding to a two-meter free fall velocity. In order to evaluate the mixing time in various locations in the ladle, nine monitoring points are chosen in the domain including the sampling location as shown in Figure 3.

The top surface boundary condition depends on the region, as shown in Figure 4. One region is covered with slag, and the other is the slag-free eye above the plume region. The 1,000mm diameter circle region directly above the porous plug is assumed as the plume region. The boundary conditions are as follows.

Plume region (no slag): Free shear condition

$$\tau_{xy} = \tau_{yz} = 0, u_y = 0 \tag{25}$$

Covered region (with slag): No slip condition

$$\underline{u} = 0 \tag{26}$$

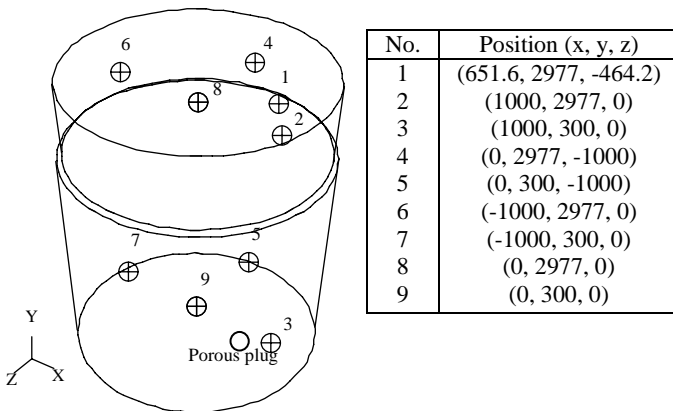| No.	Position (x, y, z)
1	(651.6, 2977, -464.2)
2	(1000, 2977, 0)
3	(1000, 300, 0)
4	(0, 2977, -1000)
5	(0, 300, -1000)
6	(-1000, 2977, 0)
7	(-1000, 300, 0)
8	(0, 2977, 0)
9	(0, 300, 0)

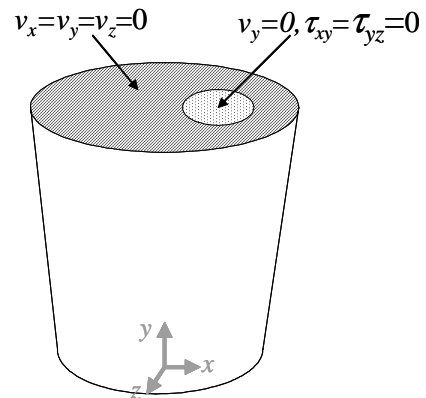Figure 3 Monitoring locations inside ladle

Figure 4 Boundary condition at the top surface showing eye caused by plume moving away slag cover

The boundary conditions on the side and the bottom walls are set to the no slip condition, $\underline{u}$=0.
The list of constants is shown in Table V.

Table V List of constants

Property	Symbol	Value	Unit
Specific heat of liquid steel	C_{pM}	820	J/kg·K
Specific heat of SiMn	C_{pA}	845.7	J/kg·K
Diffusion coefficient manganese in liquid steel	D_M	5.5×10^{-5}	m²/s
Gravitational acceleration	g	9.8	m/s²
Thermal conductivity of liquid steel	k_M	40.3	J/m·s·K
Initial temperature of SiMn	T_0	293	K
Liquidus temperature of steel	T_s	1803	K
Viscosity of liquid steel	μ	0.0067	Pa·s
Density of liquid steel	ρ	7,000	kg/m³
Density of SiMn	ρ_A	6,120	kg/m³
Density of argon	ρ_b	1.6228	kg/m³
Surface tension of liquid steel	σ	1.4	N/m

COMPUTATIONAL DETAILS

The equations and boundary conditions described above were solved using FLUENT ver. 6.1.22.[8] The computational domain is divided into about 40,000 hexahedral cells. The second-order implicit time discretization scheme is used for the unsteady discrete-phase calculation, with a chosen time step of 0.01 second. The convergence criteria are set to 10^{-5} for the residuals of the continuity equation, the momentum equations, the transport equations of k and ε, and the transport equation of Mn.

For the multi-phase flow field calculation, an efficient algorithm was developed by combining a steady flow field calculation with an unsteady discrete phase calculation, instead of using a fully-coupled unsteady flow field and discrete-phase algorithm. In this method, the unsteady discrete phase calculation is first solved in a fixed flow field for ten seconds of argon injection. After each bubble location is updated, the steady flow field is then calculated for the fixed bubble locations, including their effect on the flow field as momentum sources. These two steps are carried out alternatively until the flow field reaches steady state, which means that the flow field has little change in two successive calculation sets. Six sets of calculations were needed to achieve this. This algorithm improved the computational time for the flow field calculation from 120 hours for the fully unsteady algorithm to only 0.9 hour, using Windows XP PC with Pentium® 4 3.20GHz CPU and 2Gbyte of RAM.

For the ferroalloy calculation, a user-defined function (UDF) was developed to install the ferroalloy melting model into FLUENT. In the user-defined function, the melting time is defined as a constant. Thus, after the melting time passed from the time when each particle is introduced into the computational domain, the ferroalloy particle turns into a mass source of manganese at the particle location. It takes 8 hours to finish the 300 seconds of ferroalloy melting and mixing calculation using the same PC described above.
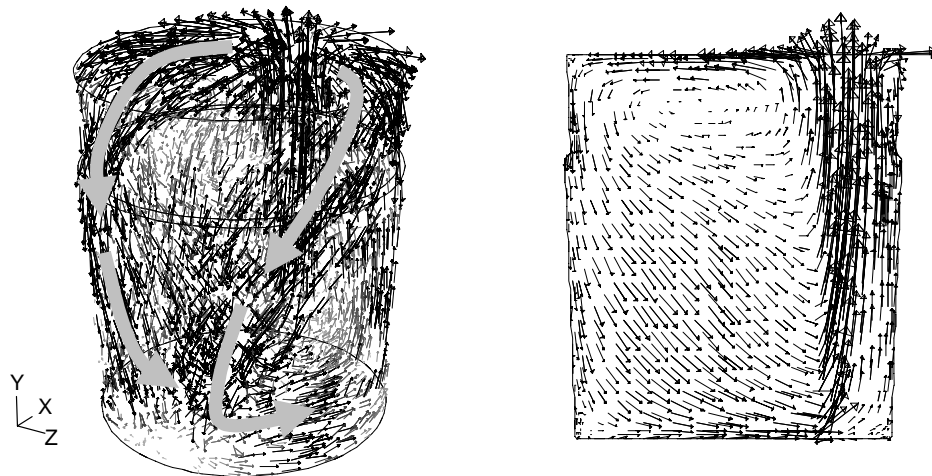
3D flow pattern   Flow in the xy centerplane
Figure 5 Calculated time-averaged flow field (FLUENT output)

Flow Field

Figure 5 shows the calculated time-averaged flow field in the steady state. The upstream jet due to bubble injection from the porous plug forms a plume that expands as it rises. The plume splits into two main streams that swirl diagonally across the top surface, flow down the far side, and converge towards the bottom corner on the opposite side of the porous plug. The returning flow pushes the plume toward the wall. The upward velocity in the plume region is given experimentally by Xie and Oeters.[9]

$$u_y^{max} = 8.64 Q_{b,V}^{0.25} \tag{27}$$

where u_y^{max} is the maximum velocity in the vertical direction in cm/s, and $Q_{b,V}$ is the volumetric gas flow rate in cm^3/s. The plume velocities from FLUENT and from equation (27) are compared in Figure 6. The computed plume velocity in this study matches well with the experimental equation (27).

Figure 7 shows the gas bubble distribution in the ladle. As it forms part of the plume, the bubble column is also pushed outward by the returning stream. There are about 1,700 bubbles (28.2mm diameter each) in the ladle under pseudo-steady state conditions, and the average bubble dwell time is 3.4 seconds.
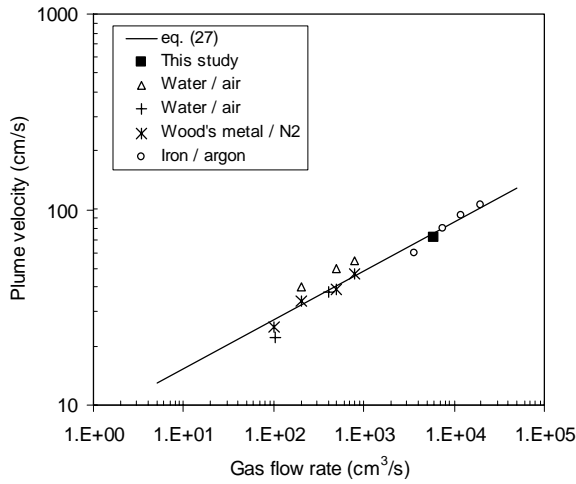

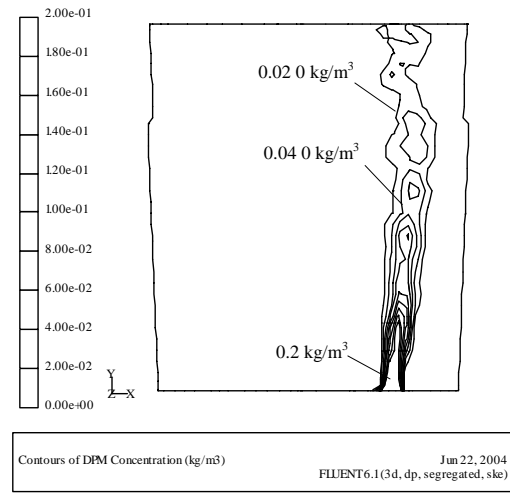Figure 6 Comparison of the plume velocity

Figure 7 Bubble distribution in the xy centerplane (FLUENT output)

Ferroalloy Melting and Mixing

Because the ferroalloys are not exactly spherical, d_A=15mm was set in equation (20) to represent the average minimum thickness of the ferroalloy particles. The relative velocity $|u-u_A|$=0.4m/s is given from the surface velocity of the computed flow field.   From the constants in Table V, equations (21) ~ (23) give Re=6269, Pr=0.1363, Nu=25.46 and h=6.84$\times10^4$ W/m^{2}K. Substituting h and other constants into equation (20), the ferroalloy melting time is obtained as follows.

$$t_1 = \frac{271}{\Delta T} \tag{29}$$

where $\Delta T = T_M - T_s$ is the superheat of the melt. The ΔT in the plant at the beginning of the operation is 20°C ~ 60°C. Thus, the ferroalloy melting time t_1 is estimated to range from 4.5 second ($\Delta T = 60°C$) to 13.6 second ($\Delta T = 20°C$).

Figure 8 shows the particle distribution during the ferroalloy addition. Because the density of SiMn is less than that of the molten steel, the ferroalloy particles float up immediately after addition, and drift along the surface just beneath the slag. They accumulate around the perimeter of the top surface opposite from the plume. Furthermore, since the ferroalloy particles reach the perimeter only 6 seconds after addition, all of the ferroalloy melting takes place in this region of the top surface perimeter. These results confirm the operational experience that ferroalloy recoveries depend on the oxygen potential of the slag, which is most likely at equilibrium with the steel at the well-mixed slag steel interface. As expected, recovery rates were strongly correlated with initial oxygen concentration during all experiments ($R^2 = 0.97$). The measured recovery of manganese ranged from 91% to 97%.
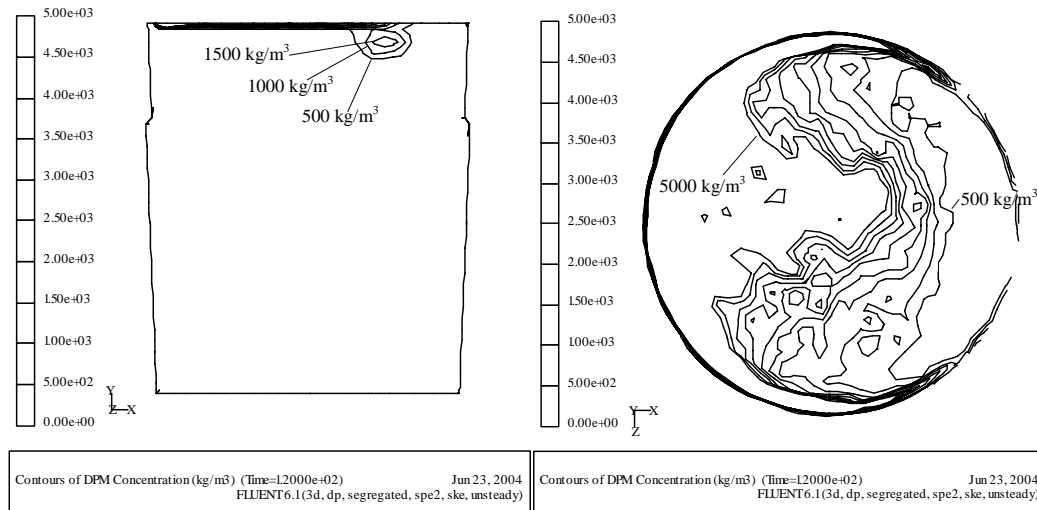
| Side view | Top View |

Figure 8 Ferroalloy particle distribution during addition (20 seconds after start of ferroalloy addition - FLUENT output)

Figure 9 shows the mixing behavior in the xy centerplane sections. The superheat for this case is 20°C and the corresponding ferroalloy melting time is 13.6 seconds. Note that solute is generated at the dense region at the top left corner where the ferroalloy particles melt. It then circulates in the ladle, and mixes by turbulent diffusion. The solute concentration finally approaches the well-mixed value of 1.26% for Heat 1.

Figure 10 compares the mixing behavior measured in the plant with the computed concentration histories at the sampling location. The normalized concentration is $(C-C_0)/(C_\infty-C_0)$, where C is the concentration at a given time, C_0 is the initial concentration, and C_∞ is the fully homogenized concentration. The two computed curves are calculated using the operational condition of Heat 1 (i.e. Q_b=0.17Nm³/s) for two superheats, 20°C and 60°C to study the effect of superheat on ferroalloy melting and corresponding mixing. The measured data from Heat 2 are also shown in comparison. However, the lower argon flow rate (Q_b=0.113Nm³/s) likely causes the longer mixing time. The computed lines reproduce the qualitative behavior of the plant data, including its oscillating nature. However, there is some difference in the peak positions, which suggests that the model may predict faster mixing than measured in the actual ladle.

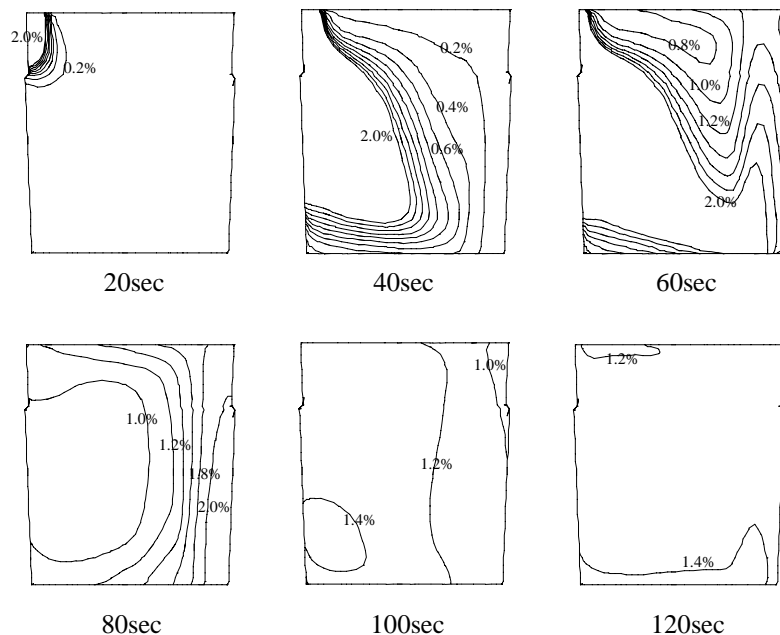| 20sec | 40sec | 60sec |
| 80sec | 100sec | 120sec |

Figure 9 Mixing behavior in the xy centerplane
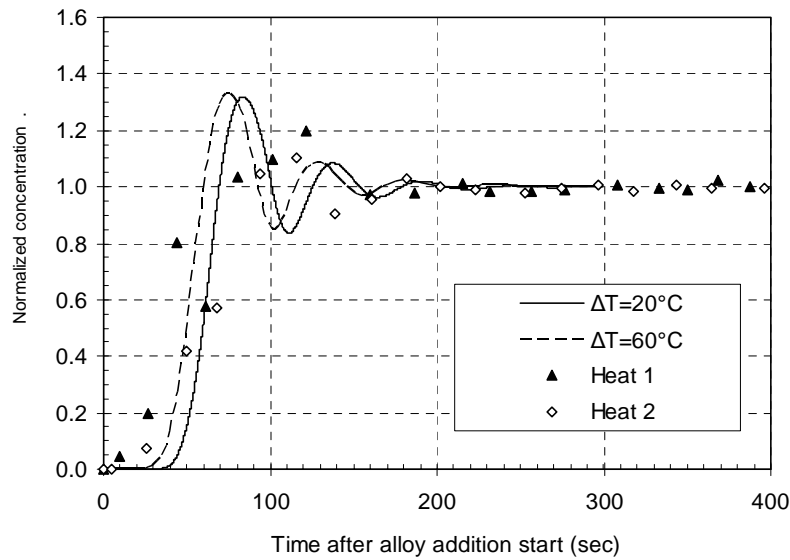(indicated time is the time after ferroalloy addition starts)

Figure 10 Computed concentration profiles at the sampling point compared with plant measurements

The variations between the measurements are likely caused also by the significant turbulent fluctuations in the molten steel, which lead to different mixing behavior depending on the local flow conditions at the instant of ferroalloy addition. This phenomenon has also been found in studies of particle motion in the continuous casting mold.[10]   In addition, the sampling location may vary slightly for each data point. A comparison of Figure 1 and 8 reveals that there is a large concentration gradient at and near the sampling location during and immediately after the ferroalloy addition. As a result, slight deviation of the sampling location could have contributed to the difference between trial and modeling data.

The results in Figure 10 also show that quantifying the mixing behavior with a mixing time to reach a given percentage (e.g. 95%) is not appropriate. This is because both the measurements and computations show that the circulating region of solute-rich fluid causes an initial concentration peak that exceeds 100% well before mixing is complete. Thus, mixing time is better defined as the time when the normalized concentration reaches 100% ± variation limits and subsequently never goes outside of this range.

Using this definition, the mixing times at various sampling points are shown in Figure 11. The mixing time was calculated for two variation limits, 1% and 5%. The location with the maximum mixing time is monitoring point 5 for ±1% and monitoring point 7 for ±5%. Thus, the region near the bottom corner of the ladle determines the mixing time needed for homogeneity of the entire molten steel heat.   The mixing times range from 88 to 187s, depending on the definition and location of mixing.   Thus, it is important to carefully choose the sampling point and then to examine the entire mixing curve.
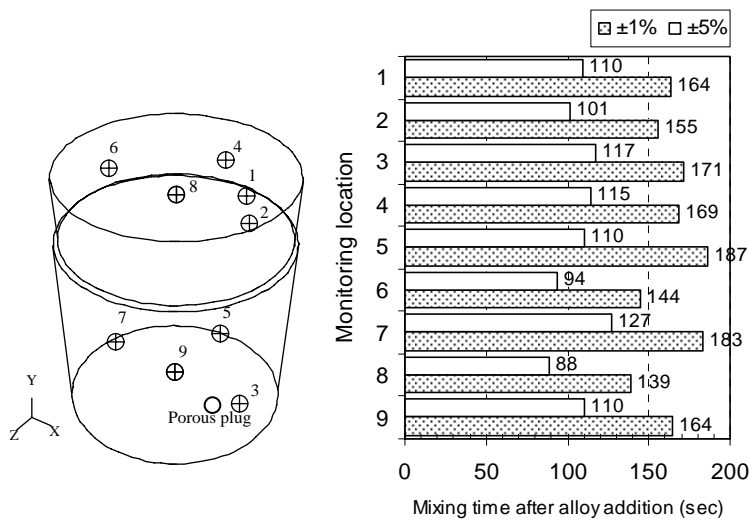

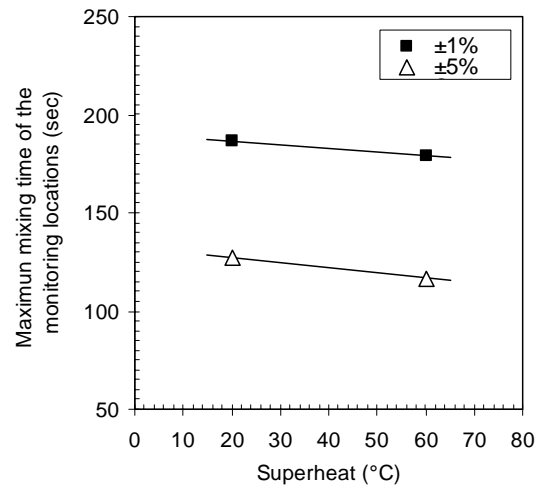Figure 11 Mixing time at various monitoring locations

Figure 12 The relationship between superheat and mixing time

Finally, the relationship between the superheat of the molten steel and the mixing time is shown in Figure 12. The maximum value of the mixing time at the nine monitoring locations is taken as the maximum mixing time. The superheat only affects the mixing times by about 10 seconds, which is the difference in the ferroalloy melting times. Thus, the mixing time mainly depends on the flow field.

CONCLUSIONS

The three-dimensional multi-phase turbulent flow field and ferroalloy mixing in an off-centered gas-stirred ladle with 130 tonne nominal capacity is investigated using plant measurements and computational models. The computed plume velocity agrees well with a previous empirical equation. A complex three-dimensional swirling flow pattern due to off-centered Ar bubbling is predicted, with about 1,700 Ar bubbles distributed in the pseudo-steady flow field.   Flow from the plume traverses the top surface, down the far walls of the ladle, and circulates back across the bottom, where it bends the plume slightly.

Alloy mixing is measured after a SiMn addition with alloy recoveries well over 90%. The SiMn melting time is from 4.5 to 13.6 seconds, according to the superheat. Computations show that the low density ferroalloy particles float quickly back to the surface of the molten steel, are transported across the ladle surface by the steel flow, and melt at the far perimeter of the ladle surface. Ferroalloy mixing behavior is simulated by coupling the melting model with a turbulent species diffusion computation in the flowing liquid. The predicted mixing behavior matches the plant measurements qualitatively, but is slightly faster. Both exhibit significant variations, with normalized concentrations that exceed 100% before mixing is complete.

Finally, mixing times depend greatly on the definition of mixing (eg. $\pm 1\%$ or $\pm 5\%$) and on the sampling location used to infer the state of mixing.   In this ladle system, mixing took 1½ to 3 minutes. This time depends mainly on the flow field and little on the ferroalloy melting time.

ACKNOWLEDGMENTS

REFERENCES

1. E. T. Turkdogan, "Equilibrium Data on Liquid Steel-Slag Reactions," *Fundamentals of Steelmaking*, The Institute of Materials, London, UK, 1996, pp. 182-183
2. A. Haider and O. Levenspiel, "Drag Coefficient and Terminal Velocity of Spherical and Nonspherical Particles," *Powder Technology*, Vol. 58, 1989, pp.63-70.
3. S. T. Johansen and F. Boysan, "Fluid Dynamics in Bubble Stirred Ladles: Part II. Mathematical Modeling," *Metallurgical Transactions B*, Vol. 19B, October 1988, pp.755-764.
4. R. M. Wellek, A. K. Agrawal and A. H. P. Skelland, "Shape of Liquid Drops Moving in Liquid Media," *A. I. Ch. E. Journal*, Vol. 12, Issue 5, 1966, pp.854-862.
5. S. A. Morsi and A. J. Alexander, "An Investigation of Particle Trajectories in Two-Phase Flow Systems," *J. Fluid Mech.*, Vol. 55, Issue 2, 1972, pp. 193-208.
6. L. Zhang and F. Oeters, "Mathematical Modeling of Alloy Melting in Steel Melts," *Steel Research*, Vol. 70, Issue 4+5, 1999, pp. 128-134.
7. S. Whitaker, "Forced Convection Heat Transfer Correlations for Flow in Pipes, Past Flat Plates, Single Cylinders, Single Spheres, and for Flow in Packed Beds and Tube Bundles," *A. I. Ch. E. Journal*, Vol. 18, Issue 2, 1972, pp. 361-371.
8. FLUENT inc., Lebanon, NH.
9. Y. Xie and F. Oeters, "Experimental Studies on the Flow Velocity of Molten Metals in a Ladle Model at Centric Gas Blowing," *Steel Research*, Vol. 63, Issue 3, 1992, pp. 93-104.
10. Q. Yuan, B. G. Thomas and S. P. Vanka, "Study of Transient Flow and Particle Transport in Continuous Steel Caster Molds: Part I. Fluid Flow,", *Metallurgical and Material Transactions B*, in press.